

Link Budget Calculation in Optical LEO Satellite Downlinks with On/Off-Keying and Large Signal Divergence – a Simplified Methodology

Dirk Giggenbach^a, Marcus T. Knopp^b, Christian Fuchs^a [v20230921]

^aInstitute of Communications and Navigation, German Aerospace Center, Oberpfaffenhofen, Germany

^bResponsive Space Cluster Competence Center (RSC³), German Aerospace Center, Oberpfaffenhofen, Germany

Abstract—Direct-to-Earth transmissions with Optical On/Off-Keying are becoming the method of choice to realize telemetry downlinks from low Earth orbit satellites at highest data-rates. Here, we review the calculation procedure for a practical assessment of the mean link budget in this space-ground data communication technology. We present a comprehensive survey of the dynamic orbital and beam-pointing effects as well as the impacts from atmospheric attenuation on the link performance. The paper provides an exhaustive review of the formulas commonly used, and propounds a recipe to reliably estimate the received power on ground. An overview of typical data transmitter terminals, transmission channel parameters, and the according optical ground stations is provided. Comparison with measured received powers over transmitter elevation angle, and the respective design estimates serves for verification.

Index Terms—Optical Satellite Downlinks, antenna gain, signal divergence, Optical Ground Station OGS, Avalanche Photo-Detector Receiver Frontend APD-RFE, satellite distance

I. INTRODUCTION

With the permanently increasing data volumes generated onboard Earth-observation satellites, as well as with the high demand of data communication in LEO (Low-Earth Orbit) Mega Constellations [1], optical transmission technologies for point-to-point communications working at multi-Gigabit-per-second data rates are getting more employed [2]. Besides optical inter-satellite links, the direct-to-Earth transmission scenario of optical LEO downlinks (OLEODL) is of major interest [3]-[10]. Standardization and optimization efforts are ongoing to enable international use between different satellite missions and Optical Ground Station (OGS) [11]-[13]. The carrier wavelengths employed today for optical Direct-to-Earth (DTE) links are in the 1550 nm region (or around 193.4 THz), using intensity-modulation direct-detection (IM/DD) signal formats. The latter allows relatively simple but still sensitive receiver technology based on Indium-Gallium-Arsenide (InGaAs) Avalanche Photodetectors (APD) [14]. Employing such bulk detectors avoids the cumbersome task of preceding atmospheric correction by Adaptive Optics (AO) techniques, as would be required for single-mode fiber coupling, to make use of pre-amplification in fiber amplifiers. Several missions have been flown or are planned to demonstrate operational OLEODLs, namely by JAXA, NICT, NASA/JPL, ESA, and DLR [15]-[21]. Optical Ground Station installations at the same time are operated by DLR, NICT, JAXA, NASA/JPL, ESA, CNES, NRL (Naval Research Lab), DSTG (Defense Science Technology Group), and more [22]-[28].

The principle of optical data downlinks implies steering the data-modulated laser-beam during downlink-phase to dynamically point towards the OGS. Such downlink contacts from LEO typically last

few to 10 minutes, depending on orbit-altitude and maximum satellite elevation, and take place only a few times per day to one OGS-location. The OGS provides a suitable receiver-antenna (namely an optical telescope), following the satellite's track in the sky. The satellite terminal's as well as the OGS' angular slew-rate can become more than $\sim 1^\circ/\text{s}$ on both ends of the link, when in zenith, requiring according angular speed and precision of the antenna control.

Optical space-downlink terminals can be classified into four categories:

- a. Passive installation of a laser-transmitter on the satellite's body, where all beam-pointing tasks must be performed by the satellite's attitude control. This task is supported by according position- and orientation-sensors, foremost the location (through a satellite-based global positioning system), and attitude-sensing by star-cameras. This poses requirements on the precision and time-delay of such sensors, however shows least impact on the satellite's structure [18].
- b. Terminals can operate an additional directional sensor for tracking an optical beacon from the OGS (like a camera or a 4-quadrant-sensor). This way, the terminals become less dependent of the satellite's attitude sensors and increase the angular precision.
- c. Active fine-control of the beam through a fast steering mirror, which is controlled directly by the attitude-sensing of a beacon from ground. The hemispherical coarse-pointing is still performed by the attitude of the satellite body. This method is most preferred when a small satellite can be rotated arbitrarily during the downlink-phase, but does not provide enough precision for a narrow laser beam to be pointed precisely [19][21].
- d. Fine- and Coarse-Pointing performed by according beacon-sensors and actuators of the laser-terminal. This is mostly required when the attitude of the whole satellite cannot be changed during a laser-downlink since the satellite is too large or must not be rotated due to other requirements [6]-[8].

The phases of one downlink contact (for terminal types b. through d.) can be separated in steps, as in Fig 1: 1, the acquisition-phase close to where the satellite rises above the horizon, where the OGS illuminates the satellite with its optical beacon, based on the direction predicted by orbital parameters. 2, when the satellite terminal detects this signal from ground with its acquisition and tracking sensor, it will orient its transmit beam to shine onto the OGS, and switch on the data

modulation. The OGS then can receive this data, and simultaneously track the satellite's (i.e. the data terminal's) position moving over the sky. 3, finally, the link is terminated when the satellite disappears close to the opposing horizon, or the signal is reduced too much by atmospheric attenuation.

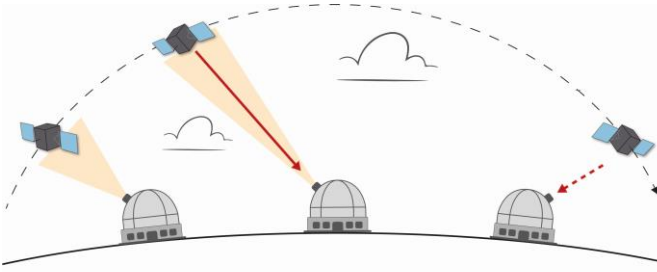


Fig. 1. Principle run of one OLEODL pass. 1. left: OGS starts by illuminating the Satellite-terminal with a broad beacon, 2. middle: then the satellite can point its narrow downlink signal onto the OGS which can follow the signal over the sky. 3. right: near the opposite horizon the link is terminated by switching off the beacon.

In the following we explain parameters and formulas for calculating the gain- and loss-effects of an optical transmitter, the communication channel, and receiver in general, we state exemplary values, and compare the analytical estimation with a measured example. We concentrate, here, on intensity-modulation with direct-detection as in “Optical On/Off-Keying” (OOK) transmission systems, which are currently being standardized in the Consultative Committee for Space Data Systems (CCSDS) [29]. The receivers use bulk (large) photo-detectors, so no adaptive optics for fiber coupling is required. Formulas presented here can partly be related to general radio-frequency satellite communication technology [5]. The optical uplink is not considered since it shows a very different behavior due to the asymmetric atmospheric channel, and the uplink is currently employed in OLEODL mainly for slow tracking purposes only.

II. BASIC CONSIDERATIONS

Fig. 2 shows the elements influencing the OLEODL performance: The satellite transmitter (a rather small optical aperture based on a lens- or mirror-telescope) sends the laser-based optical data signal towards the OGS, with a residual pointing error as small as technically possible. The distance reduces the signal intensity through beam widening, and the atmosphere perturbrates, attenuates or blocks (clouds) the laser beam and causes intensity-scintillations through its different effects [30][31]. The OGS receiver telescope finally tracks and collects the optical signal and converts it into an electrical signal through the receiver front end (RFE), where the sky's background power can reduce the performance of such a detector due to additional shot-noise current and other effects [32][33]. While optical links from/to geostationary Earth orbit (GEO) are static by nature [34], the OLEODL-scenario is highly dynamic in elevation and range, and thus imposes different and more severe challenges to maintain stable communication.

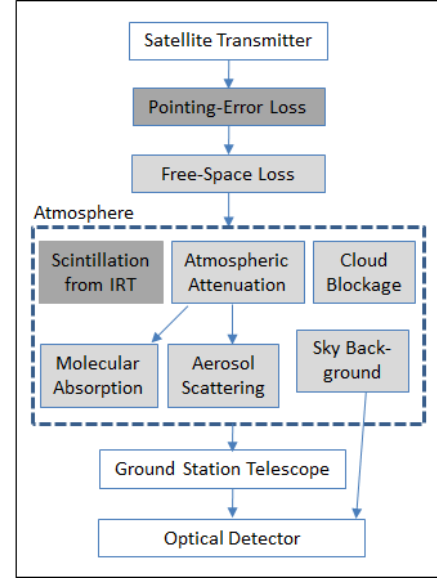


Fig. 2. Link-parameters affecting the optical downlink quality. Effects in darker boxes change faster during downlink, values in blank boxes are static.

A tracking loss at the receiver side is not mentioned in Fig. 2 since ample tracking bandwidth and a large enough photo diode area is assumed, to avoid effects from atmospheric angle-of-arrival variations and from tracking inaccuracies. However, should the detector be small compared to the receiver tracking quality, or should even single-mode coupling of the focal spot be required, then such additional loss must be regarded.

The total mean received power regarding all gains and losses can be calculated as the sum of all link budget components in dB:

$$p_{Rx} = p_{Tx} + a_{Tx} + g_{Tx} + a_{BW} + a_{FSL} + a_{Atm} + a_{Sci} + g_{Rx} + a_{Rx} \quad (1)$$

p_{Tx}	average transmit optical source power in dBm
a_{Tx}	optical power loss inside the transmitter terminal
g_{Tx}	transmitter antenna (telescope) gain
a_{BW}	average loss by dynamic beam miss-pointing and beam wander
a_{FSL}	free-space loss by link distance
a_{Atm}	sum of atmospheric attenuation effects
a_{Sci}	losses through atmospheric scintillation
g_{Rx}	receiver antenna gain
a_{Rx}	optical losses inside receiver terminal (attenuation and splitting)
p_{Rx}	received power on detector, in dBm

Logarithmic gain (g) is a positive, and attenuation (a) a negative value. The link budget calculation with values in dB or dBm is based on the basic relations between decibels-milliwatt (dBm), decibels (dB), and their linear representations A (values between 0 and 1) and G (larger than 1):

$$g_{dB} = 10 \cdot \log_{10} G \quad (2)$$

and

$$p_{dBm} = 10 \cdot \log_{10} P_{mW} \quad (3)$$

P_{mW} is the absolute mean optical power in milliwatt. The general principles for link budget calculation are elaborated in [35]-[37].

The estimated received power P_{Rx} can then be employed in a next step with the model of the RFE's sensitivity-run (compare Table III in [38] and section V.B. here). This allows calculating the instantaneous

bit error ratio (BER) of the data receiver, possibly also regarding subsequent error control processing. The latter can be forward error correction (FEC) including interleaving (for compensation of long outages by fades), or automated repeat request (ARQ) requiring bidirectional links. Such techniques, however, will not be treated in detail in this paper, as we concentrate on the run of the optical intensity and -power in cloud-free-line-of-sight (CFLOS) downlinks.

III. TRANSMITTER-INDUCED PARAMETERS

III.A. Transmitter-Antenna Gain

The linear gain $G_{Tx}(\theta, \phi)$ of a transmitting antenna in direction given through the two perpendicular angles (θ, ϕ) is defined as the ratio of the far field intensity in this direction $I(\theta, \phi)$ to the mean isotropic intensity \bar{I} . Where the latter is antenna-emitted optical signal power (after terminal-internal power losses a_{Tx}) P_0 over the full solid angle 4π .

$$G_{Tx} = \frac{I(\theta, \phi)}{\bar{I}} = 4\pi \frac{I(\theta, \phi)}{P_0} \quad (4)$$

Transmitter optics can be treated - in a first approach - similar to RF-antennas, where their far field intensity divergence angle is given through wavelength λ and transmit telescope diameter D_{Tx} . With an equally illuminated circular Tx-antenna area A , this would result in a far-field Airy pattern of intensity providing the maximum possible axial gain. In dB this would be calculated as

$$g_{Tx} = 10 \log_{10} \left(\frac{4\pi A}{\lambda^2} \right) \quad (5)$$

In practical scenarios, however, equal distribution of P_0 over A is physically impossible. The transmitter (typically fed from a single-mode fiber tip) would rather emit P_0 as a near-gaussian radial intensity distribution. At the far-field distance z (i.e. much further than the Rayleigh-distance), with e^{-2} -radius at ω_0 and lateral position r , this results in [39]-[41]

$$I(r, z) = I(0, z) \cdot e^{-2\left(\frac{r}{\omega_0(z)}\right)^2} = P_0 \frac{2}{\pi \omega_0^2(z)} e^{-2\left(\frac{r}{\omega_0(z)}\right)^2} \quad (6)$$

with $\omega_0(z) = z \cdot \frac{1}{2} \theta_{e^{-2}}$ and full intensity divergence angle $\theta_{e^{-2}}$.

Such a gaussian beam, however, cannot be transmitted uncut through the transmit telescope, since an infinitely large transmitter aperture would be required. Also, the gain (5) is the on-axis value, while further aside signal intensity and thus gain will quickly decrease according to (6). This also causes a loss related to the transmitter's pointing precision, as will later be regarded as loss from beam-wander (or jitter) a_{BW} . The influence of lateral truncation (and central obscuration, when a Cassegrain-type telescope is employed) on a gaussian beam is described in [42][43][33], resulting in an optimization of the ratio of gauss-beam versus antenna-diameter.

For simplification, often a certain ratio of the hard circular lens transmitter antenna diameter D_{Tx} to the gaussian source beam profile diameter at e^{-2} -intensity $D_{e^{-2}}$ is employed ([44], ch 4.9.2), resulting in $D_{Tx} = \sqrt{2} D_{e^{-2}} \approx 2.40 \cdot D_{FWHM}$, where we refer to a Full-Width-at-Half-Maximum (FWHM) nomenclature (meaning the beam diameter where the intensity has dropped to half of its axial maximum value).

The power of a gaussian beam inside the radial limits r is derived as

$$P(r) = P_0 \cdot \left[1 - \exp\left(-2 \frac{r^2}{\omega_0^2}\right) \right] \quad (7)$$

and we find the fraction inside this truncation-diameter $2.40 \cdot D_{FWHM}$ as 98.2% of the total beam power. The intensity relative to on-axis then becomes $e^{-4} \approx 1.8\%$. This results in a negligible truncation-loss and a far-field that can be again approximated as gaussian distribution (since the far-field transform of a gaussian beam is again gaussian).

In the scenario investigated here (a medium-divergence / small transmitter LEO-downlink) the absolute Tx-aperture size is typically not the main limiting factor, e.g. since this aperture is chosen to ensure enough power for an uplink tracking sensor. As such, the transmitter lens will always be chosen much larger than the gaussian transmit beam diameter (few centimeters or even millimeters will usually be sufficient). Then only the full divergence angle of this uncut gaussian beam must be considered. When the e^{-2} -intensity beam radius defines the collimated transmitter beam $\omega_0(0) = \frac{1}{2} D_{e^{-2}}$, the according full divergence angle $\theta_{e^{-2}}$ is

$$\theta_{e^{-2}} = 2 \frac{\lambda}{\pi \cdot \omega_0(0)} \quad (8)$$

(where a tangent function has been replaced by its argument in rad, as approximation for small angles). To relate this value to the FWHM-convention used throughout this paper, we find

$$\theta_{FWHM} = \sqrt{\frac{\ln 2}{2}} \theta_{e^{-2}} \quad (9)$$

Then the axial gain is derived as [33]

$$g_{Tx} = 10 \log_{10} \left(\frac{4\sqrt{2}}{\theta_{e^{-2}}} \right)^2 = 10 \log_{10} \left(\frac{4\sqrt{\ln 2}}{\theta_{FWHM}} \right)^2 \quad (10)$$

Table I lists transmitter-antenna properties of a selection of existing laser-terminal developments [6]-[10],[18],[21],[45].

TABLE I: PROPERTIES OF LASER TRANSMITTERS FOR DATA DOWNLINKS

Optical Data Terminal	Orbit /km	Tx data rate /Mbps	P_{Tx} /W	λ /nm	θ_{FWHM} / μ rad	Tx-gain /dB
OSIRISv1	595	39 to 622	1	1545	$\sim 1.0E3$	70.4
OSIRISv2	510	1000	1	1545	200	84.4
OSIRISv3	410	10,000	1	1560	66	94.1
OSIRIS4CUBE	520	100	0.1	1550	113	89.4
SOTA	627	1 or 10	0.03	1550	223	83.5
OPALS	410	50	2.5	1550	$\sim 1.0E3$	70.4
OCSD	450	50 to 200	2	1064	$\sim 2.0E3$	64.4
CLICK-A	400	5 to 50	0.2	1550	1.3E3	68.2

III.B. Pointing Loss from Satellite Transmitter Beam

Since the dynamic attitude control of the laser beam during a downlink pass will always bear pointing imperfections, losses caused by the axis-offset of the spot from the OGS are introduced. This loss will be dependent on the angular speed and the pointing quality of the laser terminal, as well as on the satellite's dynamic attitude information and knowledge of mechanical and electronic offsets. Pointing errors can be identified from the following causes [46]:

1) Residual attitude noise and onboard vibrations, stemming from star cameras, or pointing mechanics and inadequate sensor resolution. The effect will be a dynamic fading of the power at the OGS. Additionally, the atmospheric IRT also causes random deflections of

the beam direction, but in our case of optical downlinks with a broad beam divergence, these tend to be negligible.

2) A constant angular boresight error, where the beam-axis is at an offset angle from the target (i.e. the OGS). This will result in a constant loss from axial maximum.

3) A coordinate offset in pointing to the OGS position, when the satellite's beam points to a location at a fixed ground distance aside the OGS. The loss-effect will be higher the shorter the link distance becomes [47].

4) A dynamic angular boresight error is caused by inadequate (or missing) correction of the point-ahead-angle (PAA). The latter is the angle between incoming (data-downlink) and outgoing (beacon-uplink) beam, caused by the orthogonal relative movement of the communication partners. In LEO this PAA is typically between $\sim 20\mu\text{rad}$ at the horizon and up to $\sim 50\mu\text{rad}$ in zenith. When the satellite is tracking onto a beacon signal from the OGS without correcting for this PAA, it will be pointing aside the OGS accordingly. And when the satellite's beam has a small divergence angle (in the range of the PAA itself), this error will again cause non-negligible and elevation-dependent loss [48].

Except for 1) these effects are deterministic and can be regarded and mechanically compensated. The pointing jitter however (and also the miss-pointing by wrong attitude-knowledge, as we will see in our measured example later) will exhibit a residual dynamic fading effect. Furthermore, the pointing-ability of the satellite-terminal will be related to the strength and stability of the beacon signal received at the satellite. This signal will be hampered by atmospheric attenuation and IRT-scintillations, and, thus, will again be elevation-dependent.

Effect 1) depends on the ratio of beam-divergence versus the pointing error. When assuming this jitter radially homogeneously distributed, it can be well approximated in the far-field domain (receiver aperture is much smaller than beam-diameter) with its intensity distribution function $f_I(l) \approx \beta \cdot l^{\beta-1}$. This is a special case of the beta-distribution with one parameter β , according to (11), where $(\theta_{e-2}/2)$ is the radial $1/e^2$ beam-divergence angle and σ_{BW} is sigma of residual radial beam-wander-angle. This radial beam wander is Rayleigh-distributed [49][50]. Referring this ratio to the FWHM gaussian-beam divergence angle θ_{FWHM} results in

$$\beta = \frac{1}{2} \left(\frac{\theta_{e-2}/2}{\sigma_{BW}} \right)^2 = \frac{\theta_{FWHM}^2}{4 \cdot \ln 2 \cdot \sigma_{BW}^2} \quad (11)$$

leading to *beta-distributed* received power which implies a mean-power loss in dB of

$$a_{BW} = 10 \log_{10} \frac{\beta}{\beta+1} \quad (12)$$

The actual values for β are varying strongly, from near-negligible (i.e. a very high β) to values increasing the mean BER of the transmission significantly (where however also the sensitivity-run of the RFE's $BER(P_{Rx})$ needs to be regarded [38]).

This mean pointing loss (12) however does not reflect the additional dynamic intensity-fading effects leading to transmission-quality impairments, i.e. increase of average BER (compare section IV.C).

IV. CHANNEL PROPERTIES AND ATMOSPHERIC EFFECTS

IV.A. Elevation and Distance

The transmission channel is governed by free-space loss (FSL) due to link distance L , plus atmospheric effects. We define FSL in dB classically with the wavelength λ and distance L as

$$a_{FSL} = 10 \log_{10} \left(\frac{\lambda}{4\pi L} \right)^2 \quad (13)$$

where the loss a_{FSL} is a negative value in dB.

The angles and distances in the general triangle Satellite – Ground Station – Earth-center for a circular orbit at H_0 above Earth (with its radius R_E), with ground station at height H_{GS} above sea-level, and at link elevation angle ϵ , can directly be derived with the general triangle relations (Fig. 3) employing [51] extended with the height of the OGS above sea level, H_{GS} :

$$L = \sqrt{(R_E + H_{GS})^2 [\sin(\epsilon)]^2 + 2(H_0 - H_{GS})(R_E + H_{GS}) + (H_0 - H_{GS})^2} - (R_E + H_{GS}) \sin(\epsilon) \quad (14)$$

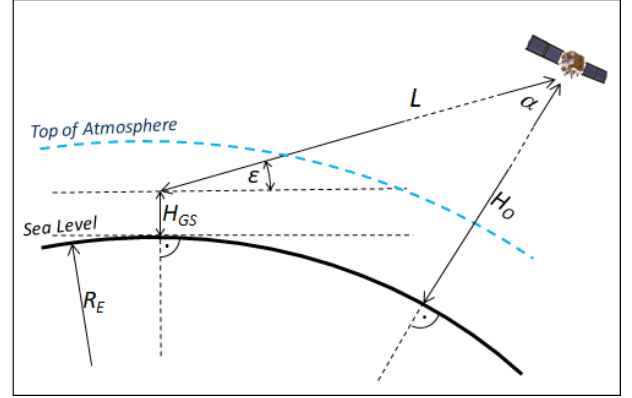


Fig. 3. Angles and distances in the general triangle Sat-GS-Earth_{center}.

Applying (14) to the typical LEO orbit at 500 km we find the distance varying from this height to 2572 km at horizon. The relative geometric FSL then ranges from 0 dB to 14.2 dB (Fig. 4).

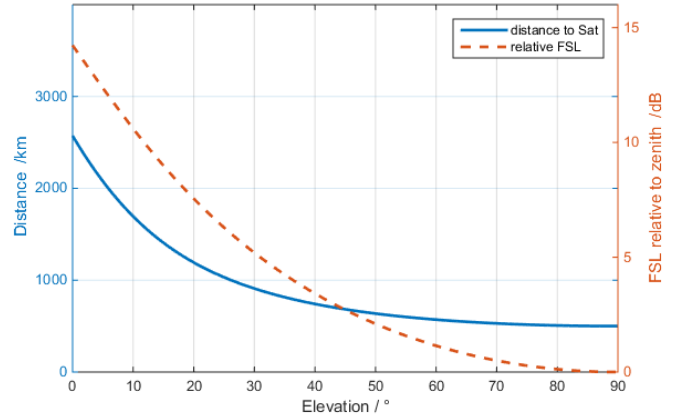


Fig. 4. Distance and relative FSL for 500km orbit height.

To communicate the occurrence of the crucial link parameter ϵ , Fig. 5 shows the typical probability density distribution of elevation for downlinks from polar orbiting LEO satellites to ground stations (here to DLR-Oberpfaffenhofen near Munich, 48.1° northern latitude), based on numerical simulations with the software from *Systems Tool Kit (STK)*. The shape of the distribution for this polar orbit height is qualitatively similar (but not identical) for other OGS-latitudes, while the absolute satellite visibility time increases when the OGS is moved from equator to pole [52],[53]. When defining 5° as the minimum elevation angle for closing a link (as is also typical in RF satellite downlinks), then 15° is the expectation value in this example, while of course 90° is the maximum.

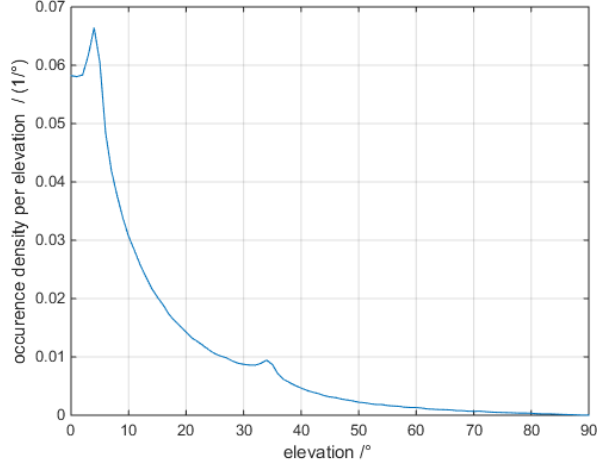


Fig. 5. Normalized distribution of link elevation occurrence in a polar LEO downlink from 500km orbit (exemplary numerical analysis).

It is often advantageous to compare directly the mean axial intensity I_0 a space-terminal generates after link distance L with a certain beam divergence, without regarding the unnecessary wavelength-parameter. This axial intensity can be calculated with (6) and (9) (not regarding atmospheric and pointing losses) as

$$I_0(L) = \frac{4 \ln 2}{\pi} \cdot \frac{P_0}{(L \cdot \theta_{FWHM})^2} \quad (15)$$

where again a gaussian far-field beam pattern is assumed.

IV.B Atmospheric Signal Attenuation

Additional loss is introduced by atmospheric aerosol-scattering and molecular absorption. By avoiding delicate spectral regions of molecular absorption lines (see Fig 9 of [30]), only aerosol absorption and scattering have to be regarded [54]. Its effect is amplified by low link elevations, since the atmospheric path becomes longer and the according attenuation is emphasized. The absorption is further influenced by the OGS-location and air-quality. In table II we state exemplary attenuation values to zenith for a favorable (first value) and a more adverse (second value) OGS-location and air quality (compare Fig. 4 of [30] for the nomenclature of atmospheric models). Derived with (10) of [30], assuming a flat-Earth model, the zenith transmission value T_z allows the calculation of the total attenuation under elevation angle ϵ

$$a_{atm} = 10 \log_{10} T_z^{1/\sin(\epsilon)} \quad (16)$$

The flat-Earth approximation is applicable for larger elevation angles and will pessimistically overestimate atmospheric attenuation at very low elevations. Exact estimates of this attenuation including the spherical-Earth geometry would require the complete absorption- and scattering-coefficients profile at all altitudes above the OGS. Such can only be estimated with the help of detailed simulations [55][30], which but actually might be missing precise initial parameters. The deviation of the flat-Earth model is due to the extension of atmospheric layers with increasing height: When this height is only close above the OGS then the extension is small, however at greater height the extension becomes relevant. As an example, the atmospheric layer 19 km to 20 km at 5° elevation is overestimated by 34% with the flat-Earth approximation, while for zero to 1 km height

it is just 1%. Since the higher atmospheric layers agglomerate volcanic aerosols, their absorption will be overestimated through (16), while any aerosols (dust / pollen) in the atmospheric boundary layer (~ below 1 km from ground) can fairly be estimated with flat-Earth modelling down to ~5° elevation. For lower elevations, the more elaborate simulation with spherical-Earth geometry should be considered, since distances tend towards infinity with a flat-Earth modelling.

Using the databases described in [30] we derive the amount of absorption above a certain height (and at wavelengths outside of molecular absorption lines), as shown in Fig. 6. Here we use for the atmospheric models exemplarily: midlatitude-summer molecular model, midlatitude-summer Rayleigh scattering, urban aerosol model, and volcanic activity level 2. Obviously, attenuation increases with shorter wavelengths, and constituents in the planetary boundary layer account for most of the total attenuation (at least as long as the volcanic absorption is not dominating).

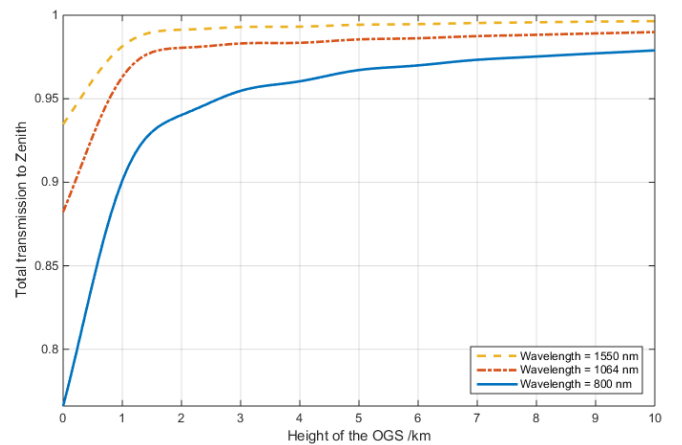


Fig. 6. Zenith transmission vs OGS altitude, acc. to models.

The plots in Fig. 6 do not regard local topographic effects like e.g. an elevated plane surrounding an OGS on a mountain top – such would resemble a typical location for an OGS (as scenario A in [30]). The first (better) values in the next table serve as a reference for this scenario A, while the other values serve as a worse-case scenario B – from sea-level and in humid tropical regions.

TABLE II: TYPICAL ATMOSPHERIC ATTENUATION TO ZENITH

wavelength /nm	OGS Altitude	Air model height-profiles of molecules / aerosols	fraction T_z to zenith
800	1km	midlatitude summer / continental clean	0.950
800	sea level	tropical / urban	0.705
1064	1km	midlatitude summer / continental clean	0.977
1064	sea level	tropical / urban	0.814
1550	1km	midlatitude summer / continental clean	0.986
1550	sea level	tropical / urban	0.891

The atmospheric attenuation loss in dB from values in Table II with (16) over elevation are plotted in Figure 7.

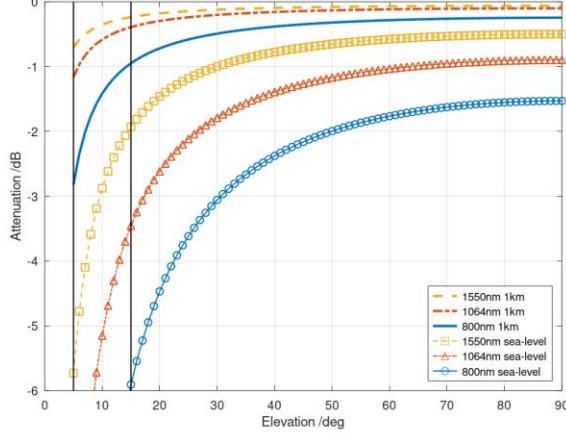


Fig. 7. Atmos. attenuation over elevation at different wavelengths, air qualities, and GS-altitudes, using flat-Earth modelling. The minimum (5°) and typical medium (15°) elevation for OLEODL are labeled as vertical lines.

IV.C. Dynamic Scintillation- and Pointing-Loss

In this representation we estimate the received power on a “mid-term” average (in our case few seconds), i.e. after effects in the millisecond domain like atmospheric scintillation or mechanical pointing jitter, but before long-term effects from link elevation changes. Additional loss stems from the nonlinear transition of instantaneous received optical power into electrical signal amplitude, which is often neglected in analysis (compare [31] and section V.B. below). Unit-mean effects do not change mean received power (since any fades are compensated by according surges at other times), but will deteriorate reception quality depending on specific implementation conditions, due to the non-linear transition from P_{Rx} to BER.

One source for such dynamic effects is the scintillation caused by atmospheric index-of-refraction turbulence (IRT), locally seized by its parameter C_n^2 . The IRT leads to phase-front distortions of the optical beam and in the further process causes so-called “speckle-patterns” of intensity by self-interference. These are quantified by the normalized variance of intensity, or *intensity-scintillation index* (ISI) σ^2 . This phenomenon is - among-others - related to wavelength, height-structure of the C_n^2 , and link distance travelled inside the turbulent atmosphere. The timescales for intensity scintillation are given through the orthogonal wind component driving the IRT-cells across the link path. Its speed is again increased by the link’s angular slew rate, prominent in OLEODLs. As the intensity’s coherence width is typically some centimeters, changes in intensity are in the milliseconds range [6].

Received optical power $P_{Rx}(t)$ is the signal intensity $I(x,t)$ integrated over the receiver-aperture. Power scintillation strength as well as its bandwidth do reduce versus intensity through the *aperture averaging effect*, which again depends on intensity structure size correlation with the aperture size. The effects of IRT on signal field quality, aperture averaging, and received signal instability are assessed in numerous publications and shall not be repeated here [44][56].

Assuming lognormal-like power distribution (which is confirmed even at low elevation angles by according measurements [31]), in [57] a threshold-based loss calculation is given. This approach can however not regard the effects of bit-interleaving and is limited to scintillation only. For a multiplication of atmospheric scintillation with pointing jitter, a joint probability density function (PDF) has been derived and verified in [58][59]. Additionally, the increase of scintillation strength with off-axis pointing of a gaussian beam up to a

maximum needs to be regarded [60], and no joined treatment for a combined PDF together with scintillation and pointing jitter is used so far.

When assuming an infinitely long bit-interleaver (ILV) before the transmitter output, the long outages due to channel-fading (i.e. the according bit error clusters) become distributed evenly after de-interleaving in the receiver, allowing the application of standard FEC-techniques to recover bit errors. Once a unit-mean distribution for received power $p(P_{Rx})$ has been defined, the unconditional long term mean error ratio $\langle BER \rangle$ is derived from its product with the BER-dependency (compare section V.B, according to (ch. 11.4.3 of [44]):

$$\langle BER \rangle = \int_0^\infty p(P_{Rx}) \cdot BER(P_{Rx}) dP_{Rx} \quad (17)$$

As a realistic assumption, the ILV should have a length of more than twenty times the channel coherence length (which is typically 5 milliseconds) to come sufficiently close to the asymptotic domain. Depending on data rate, this might require a memory of several Gigabits.

In the further run of this paper, we concentrate on the mean received power (where *mean* refers to the average of some seconds), neglecting the fast unit-mean variations from atmospheric scintillation, and the fast fades from beam jitter.

IV.D. Turbulent Beam-Spread and -Wander

Atmospheric turbulence will also lead to short-term spreading of the spot radius W_{ST} in the downlink, as well as to beam-wander of the centroid movement r_c of this spread beam - with its standard deviation $\sqrt{\langle r_c^2 \rangle}$. The latter effect will cause an additional loss in mean intensity if not tracked, similar to residual beam wander as described in section III.B. Both effects are assumed to have long-term gaussian intensity profiles and sum up geometrically, and so the long-term beam radius W_{LT} becomes $\sqrt{W_{ST}^2 + \langle r_c^2 \rangle}$. The amount of these effects depends on the weighted integral of IRT along the atmospheric link-fraction (thus, on elevation angle, wavelength, and strength of the C_n^2 profile). The beam-wander loss, i.e. the axial intensity of the atmospherically wandering beam vs its diffraction limited intensity, also depends on the initial beam divergence, meaning that a larger beam is less affected than a narrow one.

With the theoretical background as in [44] and [61], in satellite-downlinks we find additional IRT spreading angles of only few microradians even at low elevations / long atmospheric path fractions. This means that with a beam divergence of larger than 100 μ rad (as often found in OLEODL-scenarios), the effect becomes negligible. However, for even smaller divergence angles (as with large space transmitter apertures), it should be considered. Also, in optical up-links with small divergence the situation changes since the IRT-effects happen at the beginning of the link, and the turbulent beam-spread and -wander must be included in link budget calculations.

IV.E. Background Light

Optical power from *sky background radiation* through excited atmospheric molecules and aerosols (from sunlight) can impact the receiver frontend sensitivity through additional shot-noise and DC signal offset. Since a multitude of practical parameters can influence such background (e.g. field-of-view of the detector, type of receiver, spectral filtering, modulation format, sun-position, time-of-day, air-quality, ...), we do not regard these effects here, but refer to the according literature [32][62]. As an exemplary daytime-value we find

50nW of background light, leading to -3dB of loss in an APD-receiver [14]. This value can be further controlled by denser chromatic filtering and reduction of the detector's field-of-view, as far as signal spectrum and tracking system allow.

V. GROUND RECEIVER

V.A. Rx-Antenna Gain

The receiver antenna is typically a Cassegrain-type mirror telescope, and for direct-detection receivers and with the assumption $A_{Rx} <$ signal spot size its gain can be calculated by the intensity-collecting aperture area A_{Rx} :

$$g_{Rx} = 10 \log_{10} \left(\frac{4\pi \cdot A_{Rx}}{\lambda^2} \right) \quad (18)$$

with g_{Rx} as a positive value in dB [63]. When calculating the area of a Cassegrain-type telescope, the subtraction of the inner obscuration must be regarded. For OLEODL we can assume a large enough distance to the transmitter so the spot size is large and field amplitude is regarded equal over the whole receiving aperture. The reference to a *photon-collecting direct detection receiver* here implies that no diffraction-limited field effects of the atmospherically distorted signal wave front need to be regarded. I.e., no heterodyning with a local oscillator beam profile, or coupling into a single-mode fiber, is required (both tasks would denote further losses). Instead, the detector-size is assumed large enough to capture all light projected into the focal spot of the receiver telescope.

Parameters of some established optical ground stations (all Cassegrain-type telescopes) are listed in table III.

TABLE III: OPTICAL GROUND STATION PARAMETERS

OGS-Name, Organization	Aperture-Diameter	Aperture Area	Rx-Antenna Gain @ 1550nm
Izana-OGS, ESA	100 cm	0.79m ²	126.3 dB
OGSOP_old, DLR	40 cm	0.13m ²	118.2 dB
OGSOP-NG, DLR	80 cm	0.50m ²	124.2 dB
TOGS, DLR	60 cm	0.25m ²	121.2 dB
GSOC-OGS-1, DLR	30 cm	0.05m ²	114.2 dB
OGS-Almería, DLR	60 cm	0.28m ²	121.7 dB
Nemea-OGS, KSAT	50 cm	0.20m ²	120.1 dB
IZN-1-Izana, ESA	80 cm	0.50m ²	124.2 dB
Nyukasa, JAXA	60 cm	0.25m ²	121.2 dB
Tokyo, NICT	100 cm	0.79m ²	126.3 dB
TMF, JPL	100 cm	0.79m ²	126.3 dB

IM/DD optical downlinks are governed by the ability of the receiver telescope to collect enough signal power in front of the OGS and track the received focal spot on the detector. The optical power collected by A_{Rx} (when neglecting any atmospheric and systematic effects) can be estimated from the three link parameters g_{Tx} , a_{FSL} , and g_{Rx} , in one term, where the wavelength-dependency cancels:

$$p_{A_{Rx}} = p_{Tx} + g_{Tx} + a_{FSL} + g_{Rx} = p_{Tx} + 10 \log_{10} \left(\frac{4 \cdot \ln 2}{\pi} \cdot \frac{A_{Rx}}{(L \cdot \theta_{FWHM})^2} \right) \quad (19)$$

V.B. Data Receiver Sensitivity and Forward Error Correction

Optical On/Off-Keying (O3K) RFEs are often based on APDs due to their relatively simple operation while still showing ~10dB sensitivity gain compared to standard thermal-limited positive-intrinsic-negative semiconductor (PIN) receivers [64]. The simple P_{Q2} parameter-model $Q(\bar{P}_{Rx}) = 2 \cdot (\bar{P}_{Rx} / \bar{P}_{Q=2})^n$ allows calculation of any required data-signal power from a reference value at quality-factor $Q=2$ (or a BER of 0.023) and regarding the exponent of the sensitivity-run [38]. Relation

between Q and BER in an O3K-receiver is $BER = 0.5 \cdot \text{erfc}(Q/\sqrt{2})$. Table IV summarizes various measured RFE sensitivities, stating necessary mean signal power values for P_{Q2} and also for $BER=10^{-3}$. The latter BER-value would be sufficient together with a standard Forward Error Correction (FEC) code (here using the Reed-Solomon code RS(255,223) as described in [65] [66]), to achieve near-errorless data reception quality as shown in Fig. 8: Here the uncoded BER-run of the bare "APD-RFE300M" from Table IV with white-gaussian-noise (no fading) is used exemplarily, and compared with the according FEC-word-error-rate (WER) after decoding. Independent of this specific RFE's sensitivity run, we acknowledge the connection of a channel-BER= 10^{-3} sufficient to provide a practically error-free bit stream after decoding (WER< 10^{-10}). The WER-curve accounts all uncorrectable FEC words as 100% erroneous bits. This proceeding is rather conservative when recognizing that also uncorrectable packets still hold useful information that might be retrieved with alternative algorithms.

The introduction of a so-called "coding gain" is not necessary with our approach. Such a value would anyway be ambiguous since its magnitude depends on a target BER of a particular transmission system, and cannot be generalized.

A rather small throughput-loss has to be accepted with RS(255,223) since the code requires a parity overhead of $1 - 223/255 \triangleq 12.5\%$. Other FEC-codes do offer more error-correction capability, however require more parity and thus throughput-loss. Here we assume this type of FEC exemplarily since it will also be standardized in the "CCSDS Blue Book on Optical On-Off-Keying - Synchronization and Coding" (to be published). A detailed treatment of error-correction techniques can be found in various literature.

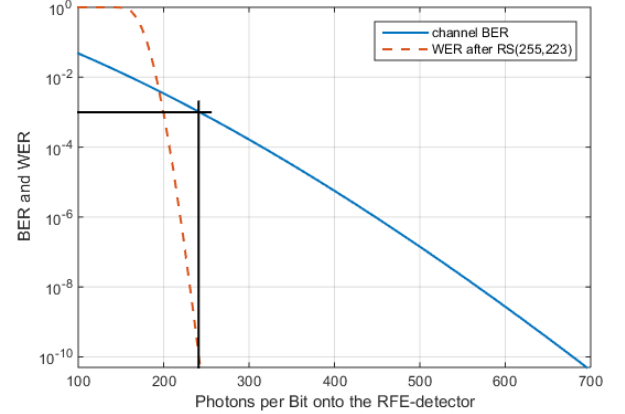


Fig. 8. Channel-BER and FEC-WER: after decoding with RS(255,223) the WER reaches 10^{-10} , when the uncoded reception is only $BER=10^{-3}$.

Besides the rather simple but efficient APD-technology, RFEs might also be based on photon-counting superconducting nanowire detectors [67], or coherent receivers with preamplification. Such, however, pose much higher technological challenges than APD-RFEs and are not considered here.

From the required power P_{1E-3} for $BER=10^{-3}$ (i.e. $Q=3.1$) (compare Table IV second-last column), we derive the value in dBm according to (3), for use in the link budget estimation Table V. While Table IV states measurements of real-world RFE-implementations, for optimized APD-RFE designs a typical sensitivity is 250 Photons/bit at signal wavelength $\lambda=1550nm$ and for any data rate R . The required signal power is

$$P_{1E-3} = 250/bit \cdot R \cdot \frac{hc}{\lambda} \quad (20)$$

with $c=2.998E8$ m/s, $h=6.626E-34$ Ws².

TABLE IV: SENSITIVITY OF FREE-SPACE INGAAS-APD DATA RECEIVERS

RFE	detect. diam.	test data rate	P_{Q2}	model exponent n	P_{1E-3}	Phot /bit
APD-RFE100M	200 μm	125 Mbps	5.1 nW	0.69	9.6 nW	596
APD-RFE300M	200 μm	300 Mbps	5.0 nW	0.70	9.3 nW	241
APD-RFE1G	200 μm	1.25 Gbps	28 nW	0.57	60 nW	374

Tested with InGaAs-APDs at 1550 nm wavelength; all measured without background light. Last column is mean photons per bit for $\text{BER}=10^{-3}$ as necessary before applying RS(255,223)-decoding [38][14].

VI. LINKBUDGET CALCULATION AND MEASUREMENT

As an example, for a type a) terminal OLEODL we demonstrate the total link budget by employing the foregoing formulas and concepts in table V [68]. The signal is received by the 30cm aperture of GSOC-OGS, with a SOFA attached (Small Optical ground station Focal-optics Assembly) [69]. Further technical attenuation inside the OGS to the APD-detector, by surface reflections, absorption, and power splitting for a tracking sensor, are accounted for by “Rx-internal losses -4.1dB”.

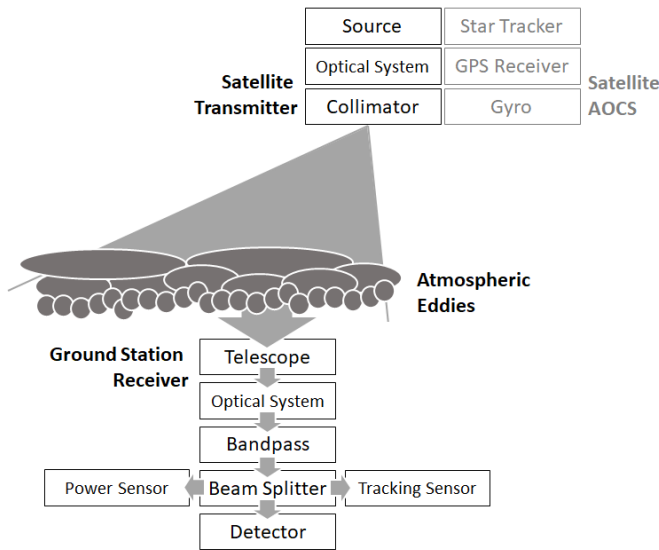


Fig. 9. Setup of OGS-telescope and SOFA as in the signal reception from OSIRISv1. After system losses and splitting to Tracking- and Sensor the RFE sees -4.1dB of all received light at 1550nm signal wavelength.

Following Table V, the link margin can be calculated for any other downlink elevation. Loss from imperfect attitude control is accounted here as “pointing loss”. No loss from atmospheric scintillation is assumed since the averaging time-window of 100ms equalized all short-term unit-mean power variations from IRT.

The results are compared in Fig. 10 with the signal power onto a data RFE, as was back-calculated from a separate power measurement (part of the received signal was split onto a power meter). These data were measured on 20th Oct 2021 with the signal from OSIRISv1 on Flying Laptop satellite to the 30cm OGS of GSOC, placed at DLR-Oberpfaffenhofen near Munich. Fast and unit-mean power variations from atmospheric scintillations are cancelled in these measured data by an averaging window of 100 ms.

TABLE V: EXEMPLARY LINK BUDGET

Parameter (formula)	OSIRISv1 on Flying Laptop satellite: 595km polar orbit, 1.0 mrad FWHM Tx-div., 1 W Tx-power of $\lambda=1550$ nm, 39 Mbps on/off keying, into “GSOC-OGS-1”	
	30° elevation	zenith
mean source power P_{Tx}	+30 dBm	
Tx internal losses a_{Tx}	-1 dB	
Tx antenna gain g_{Tx} (10)	+70.4 dB	
pointing loss a_{BW} (12)	-3 dB	
distance L (14)	1065 km	595 km
freespace loss a_{rsl} (13)	-258.7 dB	-253.7 dB
atmos. attenuation a_{atm} (16) for zenith transmission is 0.89	-1.0 dB	-0.50 dB
scintillation loss a_{sc}	NA	NA
Rx antenna gain g_{Rx} (18)	+114.2 dB	
Power into Rx aperture p_{ARx}	-49.1 dBm	-43.5 dBm
Rx-internal losses and signal splitting for tracking a_{Rx}	-4.1 dB	
p_{Rx} onto OOK data detector 250Ppb@ $\text{BER}=10^{-3}$, 39Mbps (20)	-53.2 dBm	-47.6 dBm
Link margin for communication	+5.9 dB	+11.4 dB

The theoretical plot of signal power onto the RFE (solid line) does not include a mean pointing loss, while the dashed line regards a mean pointing loss of -3dB and the measured data shows strong variations and mean losses stemming from imperfect and unstable pointing from the satellite. The OGS was never illuminated axially during this downlink, as was also verified in [70], rather a pointing offset at the FWHM-diameter of the beam was observed. Such errors are mostly due to the high rotation speed requirements for the satellite during the downlink, which can become up to 1°/s in zenith, challenging the conventional star-cameras and attitude control. Fast pointing-jitter due to vibrations - on the other hand - is negligible since the signal divergence (with 1.0 mrad FWHM) was much broader than any fast mechanical jitter.

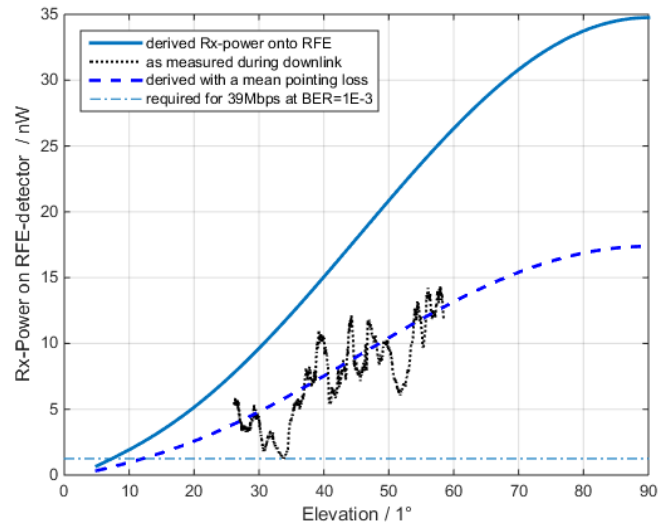


Fig. 10. Link budget of OSIRISv1 on Flying-Laptop downlinks to GSOC-OGS-1: Power onto RFE assuming perfect axial pointing (solid line), measured RFE-power showing additional loss from mis-pointing (dotted line), and power when assuming -3dB pointing loss (dashed).

From the analytical plots of Fig. 10 we read a typical mean range of the received intensity from 5° elevation (0.7 nW) to zenith (35 nW) by a factor of 17 dB, without regarding further loss from scintillation. Comparing with Fig. 5, we understand the importance to also serve very low link angles for enabling a suitable overall satellite access fraction. Such elevations however require a much lower symbol rate to work at similar energy per bit. Therefore, techniques of variable coding and modulation, or just symbol rate adaptation (variable data rate, VDR), are required [71]. Such proceeding can already be found in according standardization approaches [12].

VII. CONCLUSIONS

With optical Direct-to-Earth communication progressing towards becoming a standard transmission technique for remote sensing and reconnaissance space missions, the benefit of a uniform method for link budget calculation is getting obvious. Here, we have summarized all essential factors influencing free-space optical communications from low Earth orbiting spacecraft to ground-based receiving stations, and have presented a recipe for the assessment of the received power from the transmitter power. Considering the relevant literature of the past decades, we have based this link budget calculation specification on practical experience and verified our theoretical assessment with measured data from a real mission.

Pointing jitter from mechanical vibrations proved a rather irrelevant loss parameter in our exemplary scenario of OSIRIS-v1 downlinks, because the beam divergence was much larger than such vibration amplitudes. This should be different with future smaller-divergence terminals. However, the orbital miss-pointing of the satellite here could be interpreted as pointing jitter, and an according loss can be estimated.

A systematic loss from atmospheric scintillations depends on the complete OGS-setup including aperture-size, receiver-type, and data processing like interleaving with error correction. With ample telescope-size and perfect FEC-processing it might be negligible, for realistic scenarios it includes unit-mean elevation-dependent influences and requires according parameter distributions for its assessment.

Our survey will not only help newcomers to the field of free-space optical satellite communications to get started quickly, but also make the design of laser-based space-to-ground transmission systems easier for experienced engineers. As commercial products for free-space optical downlinks are booming in the market, this technology is supposed to bring a worldwide telecommunication revolution. Hence, the formulas reviewed here will contribute to standard measures for assuring comparability between different free-space optical transmission systems.

ACKNOWLEDGMENT

The authors want to thank Steffen Gaisser of University of Stuttgart for the operation of Flying Laptop during OSIRISv1-downlinks, and Andreas Immerz and Petro Karafillis of DLR-IKN and DLR-GSOC for analyzing the downlink measurements to GSOC-OGS-1.

DATA AVAILABILITY STATEMENT

The data required to reproduce the measurement in Fig. 10 can be made available on request to the authors.

SYMBOLS AND ABBREVIATIONS

A_{Rx}	receiver telescope aperture area
$a_{Tx} \dots g_{Rx}$	see below formula (1)
D_{FWHM}	FWHM intensity beam diameter
I_0	axial beam intensity
L	link distance from satellite to OGS
P_{Rx}	received power onto the data-detector
P_0	emitted power from satellite antenna
$P_{Q=2}$	Received power where $Q=2$
P_{1E-3}	opt. power onto RFE detector where BER=10 ⁻³
R	data rate
r	radial coordinate
r_C	beam centroid wander
Q	Quality factor of data-reception
T_z	linear atmospheric transmission to zenith
W_{ST}	short term beam radius
β	scaling parameter of beta-distribution of beam wander
λ	wavelength
θ_{FWHM}	FWHM intensity divergence angle
$\theta_{e^{-2}}$	full divergence angle at e^{-2} intensity from axial maximum
ω_0	gaussian beam radius where Intensity dropped to e^{-2} of axial value
APD	Avalanche Photo Diode
BER	Bit-Error Ratio
CCSDS	Consultative Committee on Space Data Systems
DLR	German Aerospace Center
FWHM	Full-Width at Half of the (axial) Maximum
GSOC	German Space Operations Center
IKN	Institute of Communications and Navigation
IM/DD	Intensity Modulation Direct Detection
InGaAs	Indium Gallium Arsenide – semiconductor material
IRT	Index-of-Refraction Turbulence
ISI	Intensity-Scintillation Index
LEO	Low Earth Orbit
OGS	Optical Ground Station
OLEODL	Optical LEO Data Downlinks
O3K	Optical On/Off-Keying Modulation
Ppb	Photons per bit
RFE	Receiver Front End
SOFA	Small OGS Focal-optics Assembly
VDR	Variable Data Rate

REFERENCES

- [1] A.U. Chaudhry, H. Yanikomeroglu, "Laser Intersatellite Links in a Starlink Constellation – A Classification and Analysis", IEEE Vehicular Technology Magazine, June 2021
- [2] H. Kaushal and G. Kaddoum, "Optical Communication in Space: Challenges and Mitigation Techniques" in IEEE Communications Surveys & Tutorials, vol. 19, no. 1, pp. 57-96, First quarter 2017, doi: 10.1109/COMST.2016.2603518
- [3] D. Giggenbach, F. Moll, C. Schmidt, C. Fuchs, A. Shrestha, "Optical on-off keying data links for low Earth orbit downlink applications" Satellite Communications in the 5G Era, IET TELECOMMUNICATIONS SERIES, 79, 2018
- [4] D. Giggenbach, A. Shrestha, C. Fuchs, C. Schmidt, F. Moll, „System Aspects of Optical LEO-to-Ground Links”, International Conference on Space Optics - ICSO, 2016
- [5] International Telecommunication Union, ITU Handbook on Satellite Communications. 3rd ed. Hoboken, NJ, USA: Wiley, 2002
- [6] T. Jono, Y. Takayama, N. Perlot, D. Giggenbach, et al, "Report on DLR-JAXA Joint Experiment: The Kirari Optical Downlink to Oberpfaffenhofen (KIDOD)", JAXA and DLR, ISSN 1349-1121, 2007
- [7] N. Perlot, et al. "Results of the optical downlink experiment KIDOD from OICETS satellite to optical ground station Oberpfaffenhofen (OGS-OP)" Proc of the SPIE Vol. 6457, 2007.
- [8] D.R. Kolev, et al. "Overview of international experiment campaign with small optical transponder (SOTA)" IEEE International Conference on Space Optical Systems and Applications (ICSOS). IEEE, 2015.
- [9] D. Giggenbach, C. Fuchs, C. Schmidt, R. Jaiswal, A. Shrestha, S. Gaisser, J. Keim, "Optical Data Downlinks from OSIRIS on Flying Laptop Satellite". 8th ESA Int. Workshop on TT&C Systems for Space Applications, 24-27 Sept 2019, Darmstadt, Germany,

- [10] T.S. Rose, et al. "Optical communications downlink from a 1.5 U CubeSat: OCSO program." International Conference on Space Optics—ICSO 2018. Vol. 11180. International Society for Optics and Photonics, 2019.
- [11] B.L. Edwards, K.-J. Schulz, et al, "An Update on the CCSDS Optical Communications Working Group", 2019 IEEE International Conference on Space Optical Systems and Applications, ICSOS 2019, Portland, Oregon, USA, 2019
- [12] P.D. Arapoglou, N. Mazzali, "System-level Benefit of Variable Data Rate in Optical LEO Direct-to Earth Links", International Conference on Space Optics ICSO 2020
- [13] D. Giggenbach, "Standards for Optical Space Communications", IEEE-SSC Newsletter, Vol. 30, December 2020
- [14] D. Giggenbach, "Free-Space Optical Data Receivers with Avalanche Detectors for Satellite Downlinks Regarding Background Light", *Sensors*, 22 (18), 2022
- [15] M. Toyoshima, K. Takizawa, T. Kuri, W. Klaus, M. Toyoda, H. Kunimori, T. Jono, Y. Takayama, N. Kura, K. Ohinata, K. Arai, and K. Shiratama, "Ground-to-OICETS laser communication experiments, Free-Space Laser Communications VI, International Society for Optics and Photonics, vol. 6304, Sep. 2006, 63040B.
- [16] A. Biswas, B. Oaida, K. S. Andrews, J. M. Kovalik, M. Abrahamson, and M. W. Wright, "Optical payload for lasercomm science (OPALS) link validation during operations from the ISS", *Free-Space Laser Communication and Atmospheric Propagation XXVII*, International Society for Optics and Photonics, vol. 9354, 2015, 93540F.
- [17] H. Takenaka, Y. Koyama, M. Akioka, D. Kolev, N. Iwakiri, H. Kunimori, A. Carrasco-Casado, Y. Munemasa, E. Okamoto, and M. Toyoshima, "In-orbit verification of small optical transponder (SOTA): Evaluation of satellite-to-ground laser communication links", *Free-Space Laser Communication and Atmospheric Propagation XXVIII*, International Society for Optics and Photonics, vol. 9739, p. 973 903, 2016
- [18] C. Fuchs, F. Moll, D. Giggenbach, C. Schmidt, J. Keim, S. Gaisser, "OSIRISv1 on Flying Laptop: Measurement Results and Outlook", 2019 IEEE International Conference on Space Optical Systems and Applications, ICSOS-2019. IEEE International Conference on Space Optical Systems and Applications, Portland, Oregon, USA, 2019
- [19] B. Rödiger, C. Menninger, C. Fuchs, L. Grillmayer, S. Arnold, C. Rochow, P. Wertz, C. Schmidt, "High data-rate optical communication payload for CubeSats," *Proc. SPIE 11506, Laser Communication and Propagation through the Atmosphere and Oceans IX*, 1150604 22 August 2020
- [20] C. Fuchs, C. Schmidt, "Update on DLR's OSIRIS program", International Conference on Space Optics — ICSO 2018; *SPIE Proc. Vol. 11180*, 2019
- [21] H. Tomio, P. Grenfell, W. Kammerer, P. Serra, et al, "Development and Testing of the Laser Transmitter and Pointing, Acquisition, and Tracking System for the CubeSat Laser Infrared Crosslink (CLICK) B/C Mission", IEEE Int. Conf. on Space Optical Systems and Applications, Kyoto, 2022
- [22] K. Saucke, C. Seiter, M. Gregory, The Tesat Transportable Adaptive Optical Ground Station, *Proc. SPIE 9739, Free-space Laser Communication and Atmospheric Propagation XXVIII*, 973906, San Francisco, USA, 2016, 15 March
- [23] F. Bennet, K. Ferguson, K. Grant, E. Kruzins, N. Rattenbury, S. Schediwy, "An Australia/New Zealand optical communications ground station network for next generation satellite communications", *Free-Space Laser Communications XXXII*, volume 11272, SPIE, 2020
- [24] M. Akioka, H. et al. "The NICT's New Optical Ground Station for Satellite Laser Communication and SOTA-SOCRATES Experiment." 14th International Conference on Space Operations. 2016.
- [25] A. Biswas, J.M. Kovalik, M.W. Wright, W.T. Roberts, M.K. Cheng, K.J. Quirk, M. Srinivasan, M.D. Shaw, K.M. Birnbaum, "LLCD operations using the Optical Communications Telescope Laboratory (OCTL)," *Proc. SPIE 8971, Free-Space Laser Communication and Atmospheric Propagation XXVI*, 89710X, March 2014
- [26] J. M. Perdignes, Z. Sodnik, H. Hauschildt, P. Sarasa, F. Porte-Proust, M. Wiegand, C. Rochow, D. Troendle, F. Heine, "The ESA's optical ground station for the EDRS-A LCT in-orbit test campaign: upgrades and test results," *Proc. SPIE 10562, International Conference on Space Optics — ICSO 2016*, 105622V, September 2017
- [27] M. Krynitz, C. Heese, M.T. Knopp, K.-J. Schulz, H. Henniger, "The European Optical Nucleus Network" 16th International Conference on Space Operations (SpaceOps 2021), 03.-05. May 2021
- [28] M. Lantschner, C. Fuchs, V. Bordeaux, D. Giggenbach, M.T. Knopp, "An Optical Ground Station for the German Space Operations Center - Status and Outlook" 8th ESA INTERNATIONAL WORKSHOP ON TRACKING, TELEMETRY AND COMMAND SYSTEMS FOR SPACE APPLICATIONS (TTC 2019), Darmstadt 24.-27. Sep. 2019
- [29] Consultative Committee for Space Data Systems (CCSDS), "OPTICAL COMMUNICATIONS PHYSICAL LAYER", RECOMMENDED STANDARD CCSDS 141.0-B-1, August 2019 and future editions
- [30] D. Giggenbach, A. Shrestha, "Atmospheric absorption and scattering impact on optical satellite-ground links", *Int J Satell Commun Network*. 07 October 2021;1-20.
- [31] D. Giggenbach, F. Moll, "Scintillation Loss in Optical Low Earth Orbit Data Downlinks with Avalanche Photodiode Receivers", *Int. Conf on Space Optical Systems*, IEEE-ICSOS, 2017
- [32] W.R. Leeb, "Degradation of signal to noise ratio in optical free space data links due to background illumination", *Applied Optics*, 28, 1989
- [33] S.G. Lambert, W. L. Casey, "Laser Communications in Space", Artech House, 1995
- [34] R. Barrios, S. Dimitrov, R. Mata Calvo, D. Giggenbach, "Link Budget Assessment for GEO Feeder Links based on Optical Technology", *International Journal of Satellite Communications and Networking*. Wiley, Vol 39 Issue 2, March/April 2021
- [35] H.T. Friis, 'A note on a simple transmission formula,' *Proc. IRE* 34, 254–256, 1946
- [36] L.B. Stotts, P. Kolodzy, A. Pike, B. Graves, D. Dougherty, J. Douglass, "Free-space optical communications link budget estimation", *Applied Optics* Vol. 49, No. 28, October 2010
- [37] J.A. Shaw, "Radiometry and the Friis transmission equation", *Am. J. Phys.* Vol. 81, No. 1, January 2013
- [38] D. Giggenbach, R. Mata-Calvo, Sensitivity Modeling of Binary Optical Receivers", *Applied Optics*, Vol. 54, No. 28, October 1, 2015
- [39] S.A. Self, "Focusing of spherical Gaussian beams," *Appl. Opt.* 22, 658-661, 1983
- [40] J. Alda, "Laser and Gaussian Beam Propagation and Transformation", *Encyclopedia of Optical Engineering*, Marcel Dekker Inc, 2003
- [41] R. Paschotta, "Gaussian beams" in the *Encyclopedia of Laser Physics and Technology*, 1. edition October 2008, Wiley-VCH, ISBN 978-3-527-40828-3, 2008
- [42] B.J. Klein, J.J. Degnan, "Optical Antenna Gain. 1: Transmitting Antennas" *Applied Optics* Vol. 13 No. 9, Sept 1974
- [43] RECOMMENDATION ITU-R S.1590 "Technical and operational characteristics of satellites operating in the range 20-375 THz", *Int Telecomm. Union*, 2002
- [44] L.C. Andrews, R.L. Phillips, "Laser Beam Propagation through Random Media", *SPIE Press*, 2005
- [45] A. Biswas, et al. "Optical payload for lasercomm science (OPALS) link validation during operations from the ISS." *Free-Space Laser Communication and Atmospheric Propagation XXVII*. Vol. 9354. International Society for Optics and Photonics SPIE, 2015.
- [46] A.M. Carrillo-Flores, D. Giggenbach, M.T. Knopp, D. Orsucci, A. Shrestha, "Effects of Pointing Errors on Intensity Losses in the Optical LEO Uplink", *Int. Conf on Space Optics, Dubrovnik*, 2022
- [47] Y. Yang, L. Tan, J. Ma, "Mutual alignment errors due to localized distortion in free-space laser communication links", *Optics Communications*, Volume 281, Issue 17, 2008, Pages 4180-4187, 2008
- [48] J. Wang, Y. Zhou, R. Bai and G. Wang, "Point-Ahead Angle and Coalignment Error Measurement Method for Free-Space Optical Communication Systems," in *Journal of Lightwave Technology*, vol. 35, no. 18, pp. 3886-3893, 15 Sept.15, 2017
- [49] R. Esposito, "Power scintillations due to the wandering of the laser beam," in *Proceedings of the IEEE*, vol. 55, no. 8, pp. 1533-1534, Aug. 1967
- [50] P.J. Titterton, "Power Reduction and Fluctuations Caused by Narrow Laser Beam Motion in the Far Field," *Appl. Opt.* 12, 423-425, 1973
- [51] Rec. ITU-R S.1257, "Analytical method to calculate visibility statistics of non-geostationary satellite orbit satellites as seen from a point on the Earth's surface", *International Telecommunication Union, Radiocommunication Bureau*, 1997
- [52] S.Y. Li, H.C. Liu, "An Analytical Model to Predict the Probability Density Function of Elevation Angles for LEO Satellite Systems", *IEEE Communication Letters*, April 2002

- [53] K.E. Crowe and R.A. Raines, "A model to describe the distribution of transmission path elevation angles to the Iridium and Globalstar satellite systems," in *IEEE Communications Letters*, vol. 3, no. 8, pp. 242-244, Aug. 1999, doi: 10.1109/4234.781008.
- [54] A. Biswas, S. Piazzolla, "The Atmospheric Channel", in "Deep Space Optical Communications", H. Hemmati, Ed., Wiley-Interscience, 2006
- [55] M. Hess, P. Koepke, I. Schult, "Optical properties of aerosols and clouds: the software package OPAC. *Bull Am Meteorol Soc.* 1998;79(5):831-844
- [56] L.C. Andrews, R.L. Phillips, C.Y. Hopen, "Aperture averaging of optical scintillations: power fluctuations and the temporal spectrum", *Waves in Random and Complex Media*, 10: 1, 53–70, 2000
- [57] D. Giggenbach, H. Henniger, "Fading-loss assessment in atmospheric free-space optical communication links with on-off keying", *Optical Engineering* 47 (4), SPIE - Optical Press, April 2008
- [58] M. Toyoshima, K. Araki, "Effects of time averaging on optical scintillation in a ground-to-satellite atmospheric propagation", *Applied Optics*, Vol. 39 / No. 12 / April 2000
- [59] M. Toyoshima, "Long-term statistics of laser beam propagation", *IEEE Transactions on Antennas and Propagation*, Vol. 53, No. 2, February 2005
- [60] L. C. Andrews and R. L. Phillips, "Recent Results on Optical Scintillation in the Presence of Beam Wander," *Proc. SPIE*, vol. 6878, pp. 687802-687802–14, 2008
- [61] L.C. Andrews, "Field Guide to Atmospheric Optics, Second Edition", SPIE-Press, 2019
- [62] D. Rollins, J. Baars, D. Bajorins, et al, "Background light environment for free-space optical terrestrial communications links", *Proc. SPIE* 4873, *Optical Wireless Communications V*, 2002
- [63] J.J. Degnan, B.J. Klein, "Optical Antenna Gain. 2: Receiving Antennas", *Applied Optics* Vol. 13 No. 12, 1974
- [64] O. Kharraz, D. Forsyth, "Performance comparisons between PIN and APD photodetectors for use in optical communication systems", *Optik*, Volume 124, Issue 13, 2013
- [65] B. Sklar, "Digital Communications – Fundamentals and Application, 2nd Edition, Chapter 8", Prentice Hall, New Jersey, 2013
- [66] Consultative Committee for Space Data Systems (CCSDS), "TM SYNCHRONIZATION AND CHANNEL CODING—SUMMARY OF CONCEPT AND RATIONALE", Informational Report - Green Book 130.1-G-3, June 2020
- [67] V. Reddy, R. Nerem, S. Woo Nam, R. Mirin, V. Verma, "Superconducting nanowire single-photon detectors with 98% system detection efficiency at 1550 nm", *Vol. 7, No. 12 / December 2020 / Optica*, OSA, 2020
- [68] D. Giggenbach, C. Fuchs, S. Schmidt, N. Rödiger, S. Gaisser, S. Klinkner, D. Phung, J. Chabé, C. Courde, N. Maurice, H. Marley, E. Samain, G. Artaud, "Downlink communication experiments with OSIRISv1 laser terminal onboard Flying Laptop satellite", *Applied Optics*, March 2022
- [69] M.T. Knopp, A. Immerz, D. Giggenbach, A. Koehler, "The Small Optical Ground Stations Focal-Optics Assembly (SOFA)", *IAC2022, Paris*, Sept 2022
- [70] D. Giggenbach, P. Karafillis, J. Rittershofer, A. Immerz, A. Spoerl, S. Gaisser, S. Klinkner, M.T. Knopp, "Transmitter Beam Bias Verification for Optical Satellite Data Downlinks with Open-Loop Pointing – the 3-OGS-Experiment", *Int. Conf. on Space Optics, Dubrovnik*, 2022
- [71] N. Perlot, T. De Cola, "Throughput Maximization of Optical LEO-Ground Links. *Free-Space Laser Communication Technologies XXIV*, San Francisco, USA, 2012